

RESEARCH ARTICLE

Optimization of Robot Milling Accuracy Based on a New Stiffness Performance Index

KE GAO^{ID}

Chang Guang Satellite Technology Company Ltd., Changchun, Jilin 130022, China

e-mail: 1766823742@qq.com

This work was supported by Chang Guang Satellite Technology Company Ltd., under Grant ZYGAFKY02024072906.

ABSTRACT The main factor limiting the widespread use of industrial robots in machining applications is the relatively low stiffness of the robot. Stiffness performance not only affects the quality of robotic milling but also affects the accuracy of the milling process. It is necessary to improve the stiffness performance in the robotic machining process. A new robot stiffness performance index is proposed to evaluate the robot stiffness in the direction normal to the surface of the workpiece to be machined. This index is based on the functional redundancy characteristics of the robot. The relationship between the redundant axis angle and the stiffness performance index at a random point in Cartesian space, and the stiffness performance index values on a random path in Cartesian space are obtained. The robot posture optimization model is established and a new robot milling posture optimization method is introduced. The experimental results prove a significant reduction in machining error and a significant increase in machining accuracy after using the proposed robotic milling posture optimization method, which proves the validity of the proposed stiffness performance index, and the robot milling posture optimization method can be widely used in the industry. Finally, the distribution of stiffness performance index is analyzed to predict the regions of better robot stiffness performance in the workbench, which can be used as a criterion before the milling operation to optimize the robot configuration to improve milling accuracy and save time.

INDEX TERMS Robotic milling, robotic redundancy characteristics, stiffness performance index, robot posture optimization model, stiffness performance distribution.

I. INTRODUCTION

In recent years, industrial robots are more and more used in many mechanical manufacturing operations such as milling [1], turning, and welding [2]. However, industrial robots are mostly used in palletizing, painting, and deburring operations due to their low stiffness and low pose repeatability (0.01 mm~0.5 mm). The stiffness of industrial robots is typically less than 1 N/ μ m compared to the stiffness of computer numerical control (CNC) machines, which is larger than 50 N/ μ m. Considering flexibility, intelligence, and low cost, industrial robots are expected to replace CNC machines in many specific fields such as aerospace [3], shipbuilding [4], [5], [6], [7], [8], and complex parts machining [9], [10], [11], [12], [13].

The associate editor coordinating the review of this manuscript and approving it for publication was Yingxiang Liu^{ID}.

To propose an index for evaluating robot stiffness performance, it is necessary to identify the joint stiffness values. Research on joint stiffness identification and modeling has been discussed in recent years. To evaluate robot joint stiffness, the analysis of robot manipulators and the enhanced stiffness modeling, as well as a method for identifying and characterizing their stiffness were described by Alici and Shirinzadeh [14]. To improve the two-dimensional manifold, two different stiffness-oriented performance indices were compared and the modeling of the 6-DOF robot stiffness was introduced by Li et al. [15] A method for identifying the joint stiffness using laser displacement sensors was presented by Cen and Melkote, [16] The robot stiffness model was established by Guo et al. [17] to improve the positional accuracy in robotic machining. The static and dynamic stiffness models were introduced by Cvitanic et al. [18], and a posture optimization method in robotic machining was proposed. Dumas et al. [19], [20] introduced a new method for stiffness

identification, which considers the effect of robot singularity on stiffness identification. Chen and Kao [21] introduced the effective stiffness matrix taking into consideration the robot links deformation. The effective stiffness matrix was based on the conservative congruence transformation (CCT).

Research on stiffness characteristics and pose optimization has been discussed in recent years. To obtain better stiffness performance, the normal stiffness performance index (NSPI) was proposed by Chen et al. [22] to evaluate the stiffness performance of the robot for a specific pose. A machining quality index was presented by Caro et al. [23] to choose the best location for the workpiece to be machined. The Jacobian condition number was used by Zargarbashi et al. [24] as a performance criterion to optimize six-degree-of-freedom robots in five-axis machining. A method for evaluating and contrasting the static and dynamic stiffness performance was presented by Slamani et al. [25] To evaluate the benchmark circle's contortion degree, the performance index using the circularity norm was proposed by Klimchik et al. [26] To optimize the robot performance, two design goals were proposed by Kucuk and Bingul [27] (i) maximize the local indices, (ii) maximize the workspace area covered by the robot manipulator.

A new robot milling posture optimization method is proposed in this paper to improve the robot milling accuracy. The stiffness model and performance index of robot stiffness are introduced in Section II. A larger stiffness performance index means less end-effector (EE) displacement. Therefore, the stiffness performance index can be used to represent deforming resistance of the end-effector (EE). In Section III, the robot posture optimization method is presented. The influence of the redundant axis on stiffness performance index is analyzed. In Section IV, the experiment procedure and discussion are described, and the distribution of stiffness performance index for a specific height plane are analyzed. Finally, the conclusion is obtained in Section V.

II. STIFFNESS MODEL AND PERFORMANCE INDEX

In this section, the stiffness model and performance index of robot stiffness are introduced. The relationship between stiffness performance index and end-effector (EE) displacement is analyzed. It proves that the stiffness performance index k_{fs} can represent the ability of EE to resist deformation.

TABLE 1. DHm parameters and joint stiffness values of the KUKA KR60-3 robot.

Link i	d_i / mm	a_{i-1} / mm	α_{i-1} / °	Joint	Stiffness (Nmm/rad) $\times 10^9$
1	815	0	0	A1	2.1977
2	0	350	-90	A2	0.8994
3	0	850	0	A3	1.1118
4	820	145	-90	A4	0.0644
5	0	0	90	A5	0.0254
6	170	0	-90	A6	0.0200

The KUKA KR60-3 robot is used as an illustrative example. The DHm parameters and the joint stiffness values of the KUKA KR60-3 robot are shown in Table 1 [28], and the link frames are presented in Figure 1.

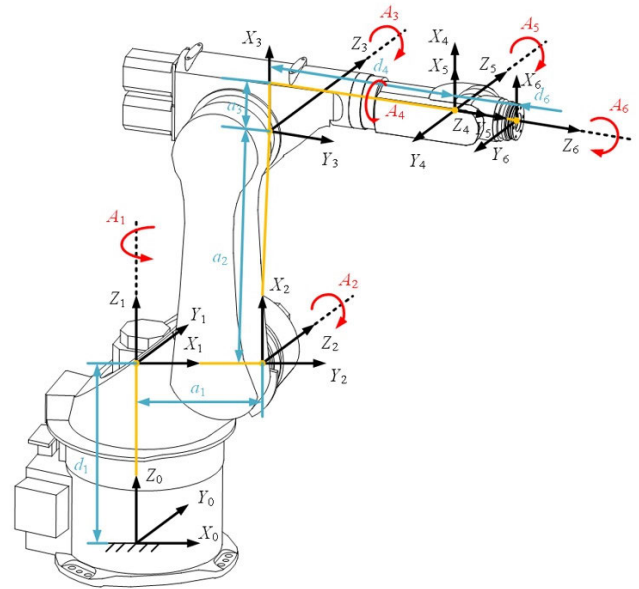


FIGURE 1. Link frames of the KUKA KR60-3 robot.

A. STIFFNESS MODEL OF ROBOT

The enhanced model introduced by Alici and Shirinzadeh [14] describes the relationship between Cartesian stiffness and joint stiffness.

$$K_X = J^{-T} (K_\theta - K_C) J^{-1} \quad (1)$$

where J is the Jacobian matrix, K_θ is the joint stiffness matrix, K_X is the Cartesian stiffness matrix and K_C is the complementary stiffness matrix (CoSM), expressed as the robot is subjected to external loading or the Jacobian changes with its configuration. K_X is more sensitive to K_θ and the impact of K_θ on K_X is much greater than that of K_C . Therefore, as long as the robot configurations are chosen appropriately, K_C can be negligible [20]. Thus equation (1) is simplified as:

$$K_X = J^{-T} K_\theta J^{-1} \quad (2)$$

The compliance matrix C is the inverse of the Cartesian stiffness matrix K_X . Therefore, the compliance matrix C can be expressed as:

$$C = J K_\theta^{-1} J^T \quad (3)$$

where C can be divided into four (3×3) submatrices as follows:

$$C = \begin{bmatrix} C_{tt} & C_{tr} \\ C_{tr}^T & C_{rr} \end{bmatrix} \quad (4)$$

where C_{tt} , C_{tr} , and C_{rr} represent the translational compliance submatrix, coupling compliance submatrix, and rotational

compliance submatrix, respectively. The end-effector (EE) rotational displacement compared to the translational displacement can be neglected because the tool radius from the workpiece surface to the tool center axis is relatively small. Thus, the translational displacement δ_t can be expressed as:

$$\delta_t = C_{tt} F_t \quad (5)$$

where $\delta_t = [\delta_x \ \delta_y \ \delta_z]^T$, and $F_t = [F_x \ F_y \ F_z]^T$ is the external forces applied on the EE.

Expanding equation (5) as

$$\begin{bmatrix} \delta_x \\ \delta_y \\ \delta_z \end{bmatrix} = \begin{bmatrix} c_{11} & c_{12} & c_{13} \\ c_{21} & c_{22} & c_{23} \\ c_{31} & c_{32} & c_{33} \end{bmatrix} \begin{bmatrix} F_x \\ F_y \\ F_z \end{bmatrix} \quad (6)$$

B. PERFORMANCE INDEX OF ROBOT STIFFNESS

Considering the unit translational displacement on the EE:

$$\|\delta_t\| = \delta_t^T \cdot \delta_t = 1 \quad (7)$$

Thus, equation (5) therefore becomes

$$F_t^T C_{tt}^T C_{tt} F_t = 1 \quad (8)$$

unit linear displacement, which means worse stiffness performance at the λ_{e2} vector direction. λ is the force required to produce a unit linear displacement in the z-axis direction. Thus, λ is the index to evaluate the stiffness performance.

Let $CC = C_{tt}^T C_{tt}$, equation (8) becomes

$$F_t^T \cdot CC \cdot F_t = 1 \quad (9)$$

namely

$$\begin{bmatrix} F_x & F_y & F_z \end{bmatrix} \begin{bmatrix} cc_{11} & cc_{12} & cc_{13} \\ cc_{21} & cc_{22} & cc_{23} \\ cc_{31} & cc_{32} & cc_{33} \end{bmatrix} \begin{bmatrix} F_x \\ F_y \\ F_z \end{bmatrix} = 1 \quad (10)$$

Expanding equation (10) as

$$cc_{11}F_x^2 + cc_{22}F_y^2 + cc_{33}F_z^2 + (cc_{12} + cc_{21})F_xF_y + (cc_{13} + cc_{31})F_xF_z + (cc_{23} + cc_{32})F_yF_z = 1 \quad (11)$$

where $F_x = 0, F_y = 0$ when we want to obtain the distance from the intersection point of the stiffness ellipsoid and the normal to the milling plane. Therefore, the stiffness performance index k_{fs} can be expressed as the length of vector λ

$$k_{fs} = \sqrt{\frac{1}{cc_{33}}} = \sqrt{\frac{1}{c_{13}^2 + c_{23}^2 + c_{33}^2}} \quad (12)$$

k_{fs} is defined as the stiffness performance index. As shown in Figure 3, the external force $F_t = [200 \ 200 \ 200]$ (N), and larger stiffness performance index values mean smaller EE displacements. Therefore, the stiffness performance index k_{fs} can represent deforming resistance of EE.

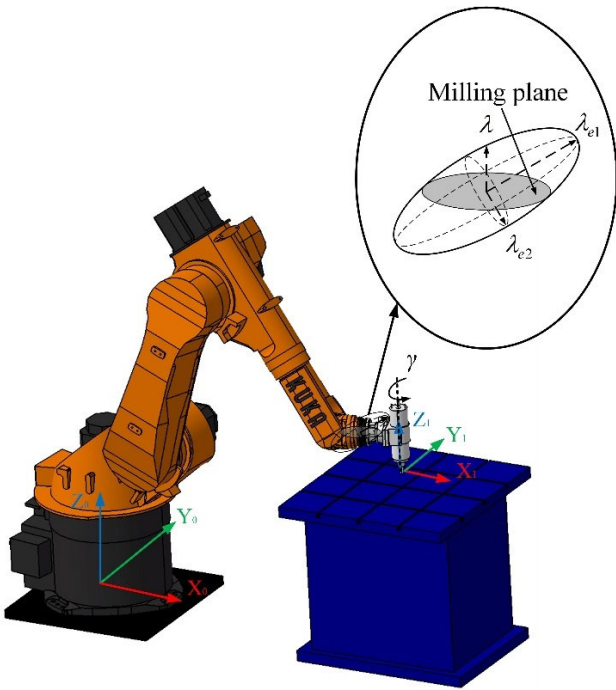


FIGURE 2. Force stiffness ellipsoid on EE and the redundant axis of the robot.

Force stiffness ellipsoid on EE is shown in Figure 2. Ellipsoid long radius λ_{e1} represents the maximum force required to produce a unit linear displacement on EE, and ellipsoid short radius λ_{e2} represents the minimum force required to produce a unit linear displacement on EE. Therefore, a larger force is required to produce the unit linear displacement, which means better stiffness performance at the λ_{e1} vector direction, and a smaller force is required to produce the

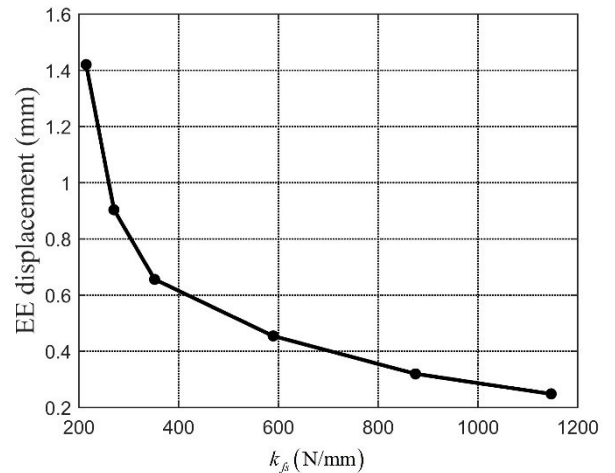


FIGURE 3. The relationship between stiffness performance index k_{fs} and EE displacement.

C. COMPARISON WITH OTHER PERFORMANCE INDICES

The normal stiffness performance index (NSPI) proposed by Chen et al. [22] and the Rayleigh quotient index proposed by Tian et al. [29] are compared with the index proposed in this paper as below.

The NSPI is defined as follows

$$k_n = \sqrt{\frac{F_{tt}^T F_{tt}}{\delta_n^2}} \quad (13)$$

where k_n is the normal stiffness performance index (NSPI), F_{tt} represents the external forces applied on the EE, and δ_n is the deformation in the surface normal direction during robotic milling. Compared to the NSPI, the stiffness performance index k_{fs} proposed in this paper represents the stiffness in the normal direction of the surface of the workpiece to be machined during the robotic milling. k_{fs} does not depend on the magnitude and direction of external forces, and is a property of the robot itself. This means that k_{fs} can be more conveniently obtained and widely applied in robot processing applications.

The Rayleigh quotient index is defined as follows:

$$R_K(d) = \sqrt{\frac{|K_{tt} \cdot d|^2}{|d|^2}} \quad (14)$$

where $R_K(d)$ is the Rayleigh quotient index, K_{tt} is the inverse matrix of the translational compliance submatrix C_{tt} , and d is the linear displacement components of the EE.

The Rayleigh quotient index $R_K(d)$ does not have directionality and cannot reflect the stiffness performance of robots in specific directions, and there is the area near the singularity of the robot's wrist with a large Rayleigh quotient index value affects the true evaluation of the robot's stiffness performance.

III. ROBOT POSTURE OPTIMIZATION

The robot posture optimization method is introduced in this section. First, robot posture optimization model is established. Then, the influence of redundant axis on stiffness performance index is analyzed. The redundant axis is shown in Figure 2. Finally, the variation of the stiffness performance index on the random path is analyzed (shown in Figure 5).

KUKA robot has six degrees of freedom, while it only takes five degrees of freedom for the robot TCP to reach most points in the Cartesian workspace, and the remaining one is redundant degrees of freedom. The redundant degrees of freedom of the serial robot rotates around the tool spindle, so when the robot is milling the same path, it can be optimized based on redundancy angles. The redundant axis angle γ is shown in Figure 2.

A. ROBOT POSTURE OPTIMIZATION MODEL

The solution of robot inverse kinematics usually contains six postures. Thus, the posture with the maximum value of the stiffness performance index is selected. In milling operations, maximizing the stiffness performance index values corresponding to redundant axis is used to optimize robot posture. With the above description, a robot posture optimization

model is established as follows:

$$\begin{cases} \max k_{fs} \\ s.t. q_{mik} = \max \text{ikine}(T(q_i)) \\ s.t. T(q_m) = T(q_{mik}, \gamma) \\ q_{i \min} \leq q_i \leq q_{i \max} \quad i = 1, \dots, 6 \end{cases} \quad (15)$$

where ikine is the inverse kinematics of the robot, T is the kinematic matrix of the robot, q_{mik} is the posture with the largest stiffness performance index among eight groups of robot inverse kinematics postures, q_i is the stiffness value of the robot joint, $i = 1, \dots, 6$, and q_m is the posture that considers the maximum stiffness performance index of robot with redundant axis angles.

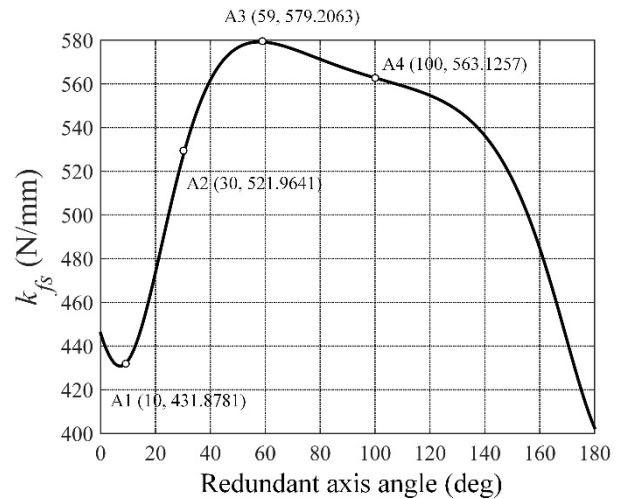


FIGURE 4. The relationship between k_{fs} and redundant axis angle for point P in the Cartesian workspace.

B. INFLUENCE OF REDUNDANT AXIS ON THE STIFFNESS PERFORMANCE INDEX

Different redundant axis angles are selected to analyze the influence of redundant axis on the stiffness performance index. As shown in Figure 4, for one point in the Cartesian workspace, the redundant axis angle has a significant effect on the stiffness performance index. It can be seen that from a redundant axis angle of 8° to 59°, the value of increases. The best stiffness performance is achieved with a redundant axis angle of 59°. As the redundant axis angle continues to increase, the stiffness performance decreases. Take point P (150, 1200, 486) mm as an example, the relationship between and redundant axis angles is shown in Figure 4.

Two points P1 (−43, 834, 486) mm and P2 (57, 947, 486) mm on the workbench are randomly selected to verify the validity of the stiffness performance index. Figure 5 shows the variation of k_{fs} values on the path from P1 to P2 for a redundant axis angle of 0°. It can be seen that from an x-axis value from −43 mm to 0 mm, the value of k_{fs} decreases. The worst stiffness performance is achieved with an x-axis value of 0 mm. As the x-axis value continues to increase, the stiffness performance increases.

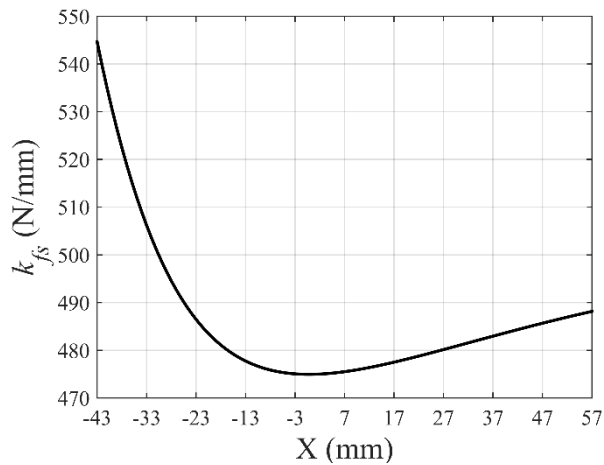


FIGURE 5. k_{fs} values on the path from P1 to P2.

IV. EXPERIMENT SETUP AND DISCUSSION

In this section, the experimental setup is first introduced. Then the relationship between stiffness performance index k_{fs} and milling error is obtained. Finally, the variation of milling error relative to k_{fs} is analyzed.

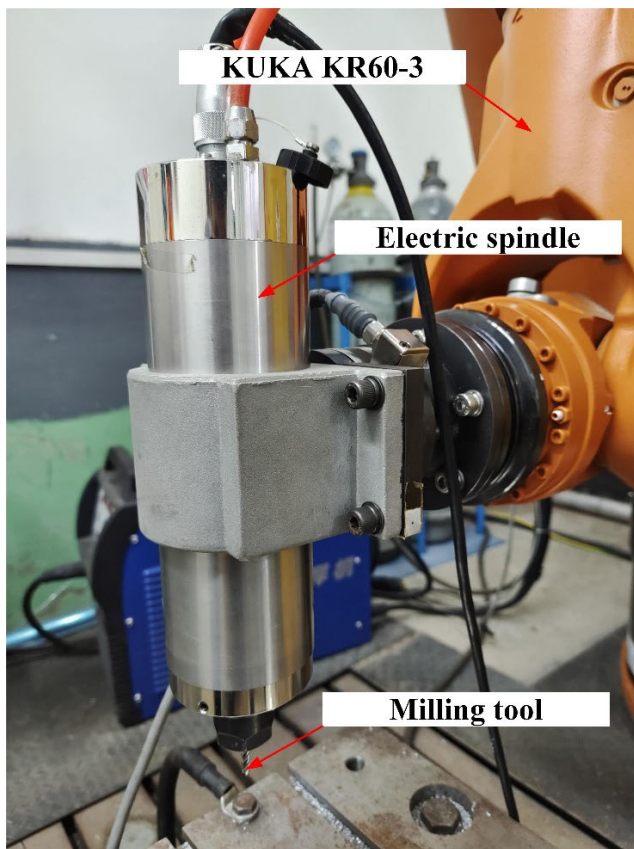


FIGURE 6. Experimental setup.

A. EXPERIMENTAL SETUP

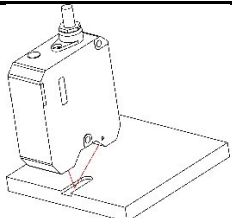
In Figure 6, the experimental system consists of a robot (KUKA KR60-3), an electric spindle, and a milling tool.

The rated power of the spindle is 2.2 kW, the rated current of the spindle is 6.4 A, and the rated speed of the spindle is 12000 rpm. The spindle is mounted on the flange of the robot. The tool parameters and cutting conditions for milling experiments are shown in Table 2. The stiffness of the robot is related to its posture, and changes in the robot's posture can cause changes in milling forces. Therefore, the robot's posture is an important factor affecting the robot's milling accuracy when the milling parameters and milling conditions remain unchanged.

TABLE 2. Tool parameters and cutting conditions for milling experiments.

Tool parameters		Milling conditions	
Materials	Tungsten steel	Spindle speed (RPM)	6000
Number of teeth	3	Feed rate (mm/s)	5
Diameter (mm)	φ8	Milling depth (mm)	0.5
		Milling mode	End
		Workpiece materials	Aluminum alloy 6061

TABLE 3. Laser displacement sensor parameters.

Measurement schematic	Keyence LK-G5000	
	Repetition accuracy (μm)	0.005
	Accuracy (%)	±0.02
	Sampling frequency (kHz)	392

B. DISCUSSION

To verify the changes of k_{fs} in Figure 4, the redundant axis angles of 10°, 30°, 59°, and 100° are selected for stiffness performance validation experiments. Given that the milling length is as small as 10 mm, it is considered that the k_{fs} value remains unchanged during the milling process. The reference surface is obtained by repeating the milling path and the measured surface is obtained by a single milling path. Therefore, the milling error can be considered as the normal distance between two surfaces. The milling error is measured by a laser displacement sensor (parameters are shown in Table 3).

Figure 7 shows the relationship between k_{fs} and milling error. Larger k_{fs} values mean higher robot stiffness in the pose, which leads to higher milling accuracy. Consistent with the above analysis, higher milling accuracy means smaller milling errors. Therefore, choosing the suitable k_{fs} can effectively improve the milling accuracy of robotic milling.

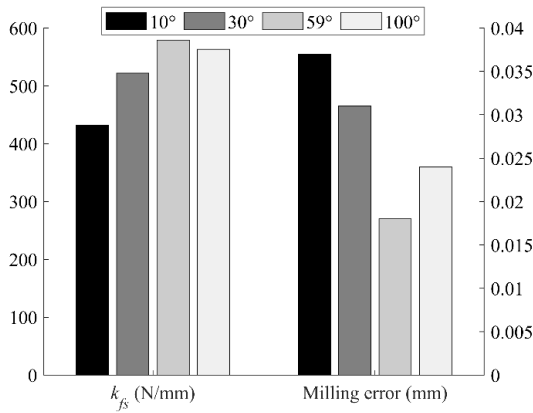


FIGURE 7. The relationship between k_{fs} and milling error.

The path from P1 to P2 is chosen to verify the variation in milling error due to changes in k_{fs} values. As shown in Figure 8, smaller milling errors represent higher milling accuracy. The milling error is consistent with the variation of k_{fs} values, which means that the proposed stiffness performance index k_{fs} can effectively reflect the accuracy of the milling process.

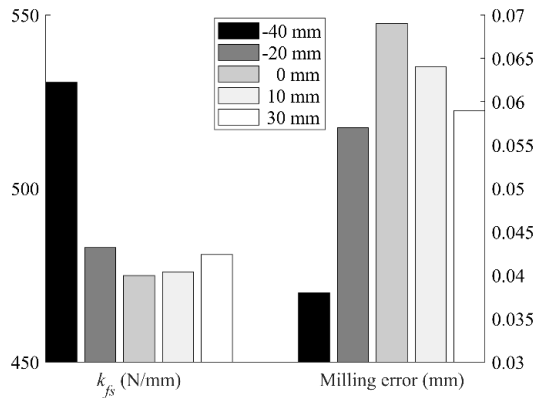


FIGURE 8. The milling error.

To further analyze the validity of the stiffness performance index k_{fs} in Figure 5, the path from P1 to P2 with different redundant axis angles is selected to verify the milling accuracy.

As shown in Figure 9, the optimization path (OP) consists of points 2 mm apart on the milling path from P1 to P2, and the robot posture at each position is the posture of the maximum stiffness performance index. The mean milling errors are consistent with the variation of the mean k_{fs} values. Therefore, the stiffness performance index k_{fs} can be used to evaluate the robot milling accuracy.

The percentage of k_{fs} values (N/mm) and milling errors (mm) is shown in Table 4. The larger milling error represents the smaller milling accuracy, and the mean milling error is also the same. For the milling path at -40 mm and 0 mm, the milling error is reduced from 0.069 mm to 0.038 mm,

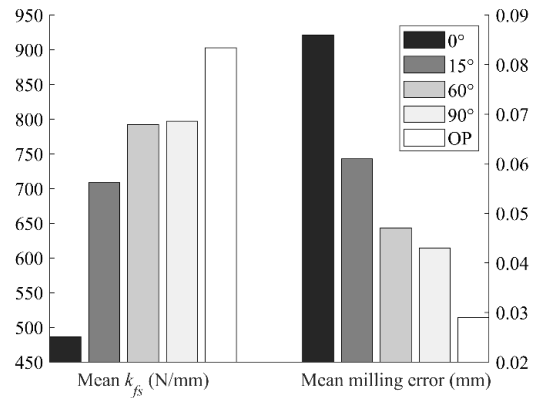


FIGURE 9. The mean milling error.

a 45.0% reduction. Consistent with the variation in k_{fs} in Figure 5, the maximum k_{fs} value (-40 mm) has the smallest milling error and the best milling accuracy, and the minimum k_{fs} value (0 mm) has the largest milling error and the worst milling accuracy. The percentage of mean k_{fs} values (N/mm) and mean milling errors (mm) is shown in Table 5. For the optimization path (OP) and the redundant axis angle of 0°, the mean milling error is reduced from 0.086 mm to 0.029 mm, a 66.3% reduction. Consistent with the variation in k_{fs} , the optimization path (maximum mean k_{fs}) has the smallest mean milling error and the best milling accuracy, and the redundant axis angle of 0° (minimum mean k_{fs}) has the largest mean milling error and the worst milling accuracy.

TABLE 4. Percentage of k_{fs} values (N/mm) and milling errors (mm).

X (mm)	k_{fs} (%)	Milling error (%)
-40	530.5647 (100%)	0.038 (55.0%)
-20	482.9829 (91.0%)	0.057 (82.6%)
0	474.9636 (89.5%)	0.069 (100%)
10	476.0073 (89.7%)	0.064 (92.8%)
30	480.9952 (90.7%)	0.059 (85.5%)

TABLE 5. Percentage of mean k_{fs} values (N/mm) and mean milling errors (mm).

Redundant axis angle (deg)	Mean k_{fs} (%)	Mean milling error (%)
0	486.2332 (53.9%)	0.086 (100%)
15	708.4366 (78.5%)	0.061 (70.9%)
60	791.8800 (87.7%)	0.047 (54.7%)
90	796.9131 (88.3%)	0.043 (50.0%)
Optimization Path	902.5687 (100%)	0.029 (33.7%)

C. DISTRIBUTION OF STIFFNESS PERFORMANCE INDEX IN THE ROBOT WORKSPACE

After obtaining the optimal redundant axis angle, the stiffness performance distribution map can be drawn by interpolating

and fitting coordinate points at 1mm intervals. It can be seen from Figure 10 that milling areas with higher values are located close to the robot base. The distribution of k_{fs} for the plane of 486 mm height is shown in Figure 10. It can be seen that the stiffness performance of the robot varies with the redundant axis angle and the position of the TCP. From Figure 10(a-c), as the red region increases in size, the stiffness of the robot increases. At a redundant axis angle of 60° , a stiffer region is shown in Figure 10(c). As the redundant axis angle continues to increase, the robot stiffness decreases. Therefore, there will always be a redundant axis angle that maximizes the stiffness of the robot on a specific plane.

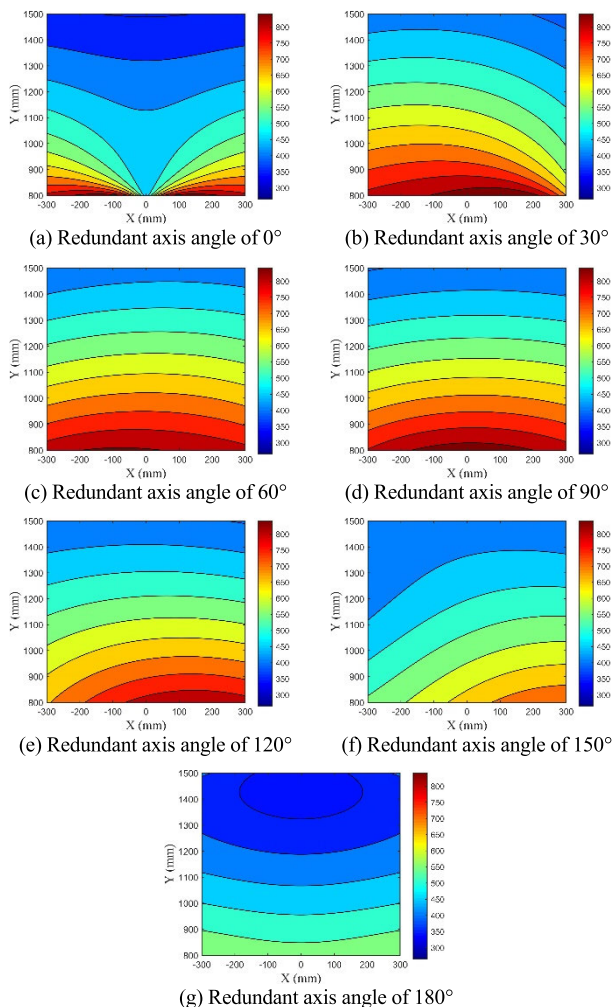


FIGURE 10. Distribution of k_{fs} for plane of 486mm height, with different redundant axis angles.

The mean, standard deviation, and PV (Peak to Valley) values of stiffness performance index k_{fs} are presented in Figure 11. Larger k_{fs} mean values reflect better stiffness performance on the workbench, and smaller k_{fs} standard deviation values reflect a smaller variation of the stiffness on the workbench. The variation in standard deviation values is small, which means the variation of the stiffness is small.

The PV values represent the dispersion of the stiffness performance index k_{fs} .

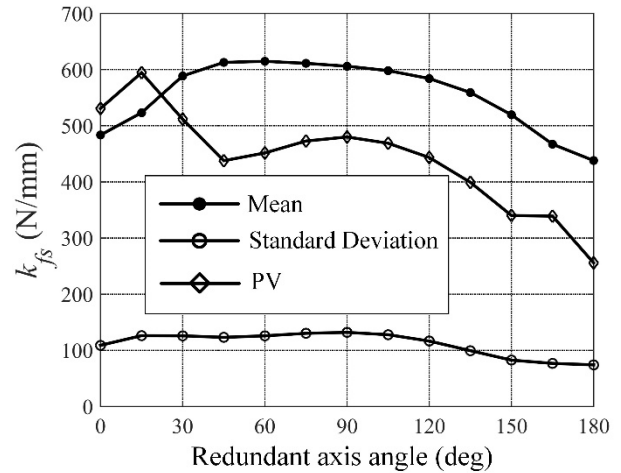


FIGURE 11. Stiffness performance index k_{fs} mean, standard deviation, and PV values.

As shown in Figure 11, the value of the standard deviation varies very little, so the standard deviation can be used not as a selection criterion to predict the region of milling accuracy. The change trend of the mean value is close to the PV value (only 15° to 45° is the opposite), which means that the dispersion is similar to the change of concentration degree. The mean value is an important criterion for reflecting the stiffness performance, so the mean value is used as the selection standard for predicting the milling accuracy area. When the redundant axis angle is equal to 60° , the mean value is maximum, which means the stiffest region. Therefore, before the milling operation, the stiffness performance distribution can be used to optimize the robot configuration, which can improve milling accuracy and save time.

V. CONCLUSION

In this paper, a new stiffness performance index k_{fs} is proposed to evaluate the robot stiffness in the direction normal to the surface of the workpiece to be machined. The index does not depend on the direction of the external force, which reduces the limitations of robotic milling and is more widely applicable to industrial applications. A milling posture optimization model based on the redundancy characteristics of the robot is proposed. This model is applicable to 6 degrees of freedom serial robots and can be extended to multi degrees of freedom robots. Then the distribution rules of k_{fs} for different redundant axis angles are presented to predict the stiffness performance distribution of robot in the workspace space. Finally, the results of milling experiments show that a larger stiffness performance index results in a smaller machining error, which means that machining errors can be reduced and machining accuracy can be improved by optimizing the redundant axis angles.

REFERENCES

- [1] H. Qu, B. Geng, B. Chen, J. Zhang, Y. Yang, L. Hu, and Y. Zhao, "Force perception and bone recognition of vertebral lamina milling by robot-assisted ultrasonic bone scalpel based on backpropagation neural network," *IEEE Access*, vol. 9, pp. 52101–52112, 2021.
- [2] Y. Zhang, J. Xiao, Z. Zhang, and H. Dong, "Intelligent design of robotic welding process parameters using learning-based methods," *IEEE Access*, vol. 10, pp. 13442–13450, 2022.
- [3] X. Wang, J. Wu, and Y. Wang, "Dynamics evaluation of 2UPU/SP parallel mechanism for a 5-DOF hybrid robot considering gravity," *Robot. Auto. Syst.*, vol. 135, Jan. 2021, Art. no. 103675.
- [4] D. Lee, "Robots in the shipbuilding industry," *Robot. Computer-Integrated Manuf., Rev.*, vol. 30, no. 5, pp. 442–450, Oct. 2014.
- [5] W.-J. Chung, K.-J. Kim, T.-J. Song, D.-Y. Kim, J.-L. Kim, M.-H. Park, and K.-S. Shin, "Simulation of an inter-block arc-welding robot for shipbuilding using a weaving motion algorithm based on a Bezier spline," in *Proc. 4th IASTED Int. Conf. Model.*, 2004, pp. 1–27.
- [6] H.-B. Chen, T. Lin, and S.-B. Chen, "The application of robotic welding in the shipbuilding," in *Proc. Int. Conf. Robotic Welding, Intell. Autom.*, 2015, pp. 1–28.
- [7] H. J. Wang, G. Q. Ding, Y. Shun, P. Q. Fiang, and G. Z. Yan, "Robot auto-marking and auto-cutting of shipbuilding panels based on a compensation algorithm," *Industrial Robot International Journal Robotics Research Application*, vol. 28, no. 5, pp. 425–433, 2001.
- [8] O. Kermorgant, "A magnetic climbing robot to perform autonomous welding in the shipbuilding industry," *Robot. Computer-Integrated Manuf.*, vol. 53, pp. 178–186, Oct. 2018.
- [9] R. Kluz and T. Trzpiecinski, "Analysis of the optimal orientation of robot gripper for an improved capability assembly process," *Robot. Auto. Syst.*, vol. 74, pp. 253–266, Dec. 2015.
- [10] Z. Wang, B. Zhou, D. Trentesaux, and A. Bekrar, "Approximate optimal method for cyclic solutions in multi-robotic cell with processing time window," *Robot. Auto. Syst.*, vol. 98, pp. 307–316, Dec. 2017.
- [11] A. Agnetis, "Scheduling no-wait robotic cells with two and three machines," *Eur. J. Oper. Res.*, vol. 123, no. 2, pp. 303–314, Jun. 2000.
- [12] C. Dumas, A. Boudelier, S. Caro, S. Garnier, M. Ritou, and B. Furet, "Development of a robotic cell for trimming of composite parts," *Mecanique Industries, Article*, vol. 12, no. 6, pp. 487–494, 2011.
- [13] C. Sriskandarajah, I. Drobouchevitch, S. P. Sethi, and R. Chandrasekaran, "Scheduling multiple parts in a robotic cell served by a dual-gripper robot," *Operations Res.*, vol. 52, no. 1, pp. 65–82, Feb. 2004.
- [14] G. Alici and B. Shirinzadeh, "Enhanced stiffness modeling, identification and characterization for robot manipulators," *IEEE Trans. Robot.*, vol. 21, no. 4, pp. 554–564, Aug. 2005.
- [15] G. Li, W. Zhu, H. Dong, and Y. Ke, "Stiffness-oriented performance indices defined on two-dimensional manifold for 6-DOF industrial robot," *Robot. Computer-Integrated Manuf.*, vol. 68, Apr. 2021, Art. no. 102076.
- [16] L. Cen and S. N. Melkote, "CCT-based mode coupling chatter avoidance in robotic milling," *J. Manuf. Processes*, vol. 29, pp. 50–61, Oct. 2017.
- [17] Y. Guo, H. Dong, and Y. Ke, "Stiffness-oriented posture optimization in robotic machining applications," *Robot. Computer-Integrated Manuf.*, vol. 35, pp. 69–76, Oct. 2015.
- [18] T. Cvitanic, V. Nguyen, and S. N. Melkote, "Pose optimization in robotic machining using static and dynamic stiffness models," *Robot. Computer-Integrated Manuf.*, vol. 66, Dec. 2020, Art. no. 101992.
- [19] C. Dumas, S. Caro, S. Garnier, and B. Furet, "Joint stiffness identification of six-revolute industrial serial robots," *Robot. Computer-Integrated Manuf.*, vol. 27, no. 4, pp. 881–888, Aug. 2011.
- [20] C. Dumas, S. Caro, M. Cherif, S. Garnier, and B. Furet, "Joint stiffness identification of industrial serial robots," *Robotica*, vol. 30, no. 4, pp. 649–659, Jul. 2012.
- [21] S.-F. Chen and I. Kao, "Conservative congruence transformation for joint and Cartesian stiffness matrices of robotic hands and fingers," *Int. J. Robot. Res.*, vol. 19, no. 9, pp. 835–847, Sep. 2000.
- [22] C. Chen, F. Peng, R. Yan, Y. Li, D. Wei, Z. Fan, X. Tang, and Z. Zhu, "Stiffness performance index based posture and feed orientation optimization in robotic milling process," *Robot. Computer-Integrated Manuf.*, vol. 55, pp. 29–40, Feb. 2019.
- [23] S. Caro, S. Garnier, B. Furet, A. Klimchik, and A. Pashkevich, "Workpiece placement optimization for machining operations with industrial robots," in *Proc. IEEE/ASME Int. Conf. Adv. Intell. Mechatronics*, Jul. 2014, pp. 1716–1721.
- [24] S. H. H. Zargarbashi, W. Khan, and J. Angeles, "The Jacobian condition number as a dexterity index in 6R machining robots," *Robot. Computer-Integrated Manuf.*, vol. 28, no. 6, pp. 694–699, Dec. 2012.
- [25] M. Slamani, A. Joubair, and I. A. Bonev, "A comparative evaluation of three industrial robots using three reference measuring techniques," *Ind. Robot, Int. J.*, vol. 42, no. 6, pp. 572–585, Oct. 2015.
- [26] A. Klimchik, A. Ambiehl, S. Garnier, B. Furet, and A. Pashkevich, "Efficiency evaluation of robots in machining applications using industrial performance measure," *Robot. Computer-Integrated Manuf.*, vol. 48, pp. 12–29, Dec. 2017.
- [27] S. Kucuk and Z. Bingul, "Comparative study of performance indices for fundamental robot manipulators," *Robot. Auto. Syst.*, vol. 54, no. 7, pp. 567–573, Jul. 2006.
- [28] K. Gao, X. Zhou, R. Wang, M. Fan, and X. He, "Joint stiffness identification based on robot configuration optimization away from singularities," *Appl. Sci.*, vol. 13, no. 8, p. 4922, Apr. 2023.
- [29] Y. Tian, B. Wang, J. Liu, F. Chen, S. Yang, W. Wang, and L. Li, "Research on layout and operational pose optimization of robot grinding system based on optimal stiffness performance," *J. Adv. Mech. Design, Syst., Manuf.*, vol. 11, no. 2, pp. JAMDSM0022–JAMDSM0022, 2017.



KE GAO received the B.Sc. degree in mechanical engineering and the Ph.D. degree in mechanical manufacturing and automation from Jilin University, Jilin, China, in 2018 and 2023, respectively. In 2024, he joined Chang Guang Satellite Technology Company Ltd., China, as a Senior Engineer of robotic manufacturing. His research interests include industrial robot automation and intelligent manufacturing.

...